JOC The Journal of Organic Chemistry

Article

pubs.acs.org/joc

Single Heteroatom Fine-Tuning of the Emissive Properties in Organoboron Complexes with 7-(Azaheteroaryl)indole Systems

Miriam Más-Montoya,[†] Laura Usea,[†] Arturo Espinosa Ferao,[†] María F. Montenegro,[‡] Carmen Ramírez de Arellano,[§] Alberto Tárraga,[†] José N. Rodríguez-López,[‡] and David Curiel*[,†]

[†]Department of Organic Chemistry, Faculty of Chemistry, University of Murcia, Campus of Espinardo, Murcia 30100, Spain

[‡]Department of Biochemistry and Molecular Biology A, School of Biology, University of Murcia, Campus of Espinardo, Murcia 30100, Spain

[§]Department of Organic Chemistry, Faculty of Pharmacy, University of Valencia, c/Vicente Andrés Estelles s/n, Burjassot 46100, Spain

Supporting Information

ABSTRACT: The application of organoboron compounds as light-absorbing or light-emitting species in areas as relevant as organic electronics or biomedicine has motivated the search for new materials which contribute to the progress of those applications. This article reports the synthesis of four-coordinate boron complexes based on the unexplored 7-(azaheteroaryl)-indole ligands. An easy synthetic approach has enabled the fine-tuning of the electronic structure of the organoboron species by modifying a heteroaromatic component in the conjugated system. Furthermore, a comprehensive characterization by X-ray diffraction, absorption and emission spectroscopy, both in solution and in the solid state, cyclic voltammetry, and computational methods has evidenced the utility of this simple strategy. Large Stokes shifts have been achieved in solid thin-films which show a range of emitted light from blue to orange. The synthesized compounds have been used as biocompatible fluorophores in cell bioimaging.

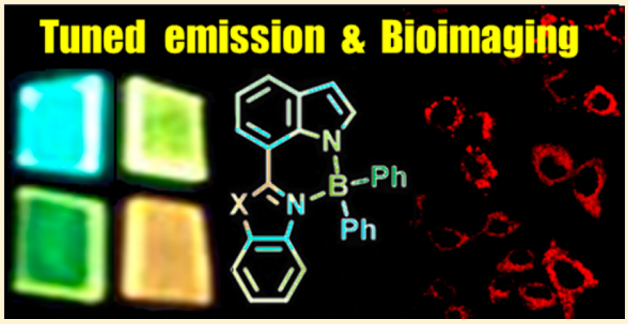

INTRODUCTION

Organoboron complexes have become very useful chromophores and fluorophores due to their applicability in relevant areas as electroluminescent devices,[1] lasers,[2] organic photovoltaics,[3] bioimaging,[4] biomedicine[5] or sensing.[6] Due to the interest in exploring new materials which adapt to the requirements of these and other applications, organic chemistry has enormously contributed to the development of innovative synthetic ligands and their boron complexes. The Bodipy structure represents one of the most attractive four-coordinate boron skeletons whose physical and chemical properties have been thoroughly studied.[7] Nevertheless, the search for alternative bidentate ligands that combine a wide variety of C−C, N−C, N−N, N−O, or O−O sites for the coordination of boron has rendered excellent results.[8] One of the main objectives in the design of these ligands aims at the achievement of tunable electronic properties through simple synthetic approaches. In this regard, the rich chemistry of indole-based compounds[9] becomes an optimum test-bench which, with a few exceptions,[10] still remains unexplored in the context of organoboron species.

Herein, we report the synthesis and comprehensive study of the luminescent properties of a family of novel 7-(azaheteroaryl)indole ligands and their corresponding four-coordinate boron complexes. The strategy to accomplish a fine modulation of the electronic structure of the π-conjugated system consists on modifying the electronic effects from structurally related heteroaromatic units such as benzoxazole, benzothiazole, benzimidazole, or pyridine.

RESULTS AND DISCUSSION

The synthesis of the ligands and complexes was carried out as depicted in Scheme 1.

Among the variety of synthetic methods for the preparation of indole derivatives, the Bartoli synthesis is especially useful to access 7-substituted indoles.[11] In this regard, using *o*-nitrobenzaldehyde and either *o*-aminophenol, *o*-aminothiophenol, or *o*-phenylenediamine as starting materials led to the isolation of 2-(2-nitrophenyl)benzoxazole, **2**, 2-(2-nitrophenyl)benzothiazole, **3**, or 2-(2-nitrophenyl)benzimidazole, **4**, respectively. An alkyl chain was attached to compound **4** to produce the *N*-octylbenzimidazole, **5**, prior to the indole synthesis. Finally, the Bartoli reaction between vinylmagnesium bromide and the nitro group in **2**, **3**, and **5** yielded the corresponding 7-(azaheteroaryl)indoles **6**, **7**, and **8**. Additionally, 7-(pyrid-2-

Received: February 5, 2016
Published: March 18, 2016

DOI: 10.1021/acs.joc.6b00265
J. Org. Chem. 2016, 81, 3296−3302

Scheme 1. Synthetic Route to Ligands and Organoboron Complexes

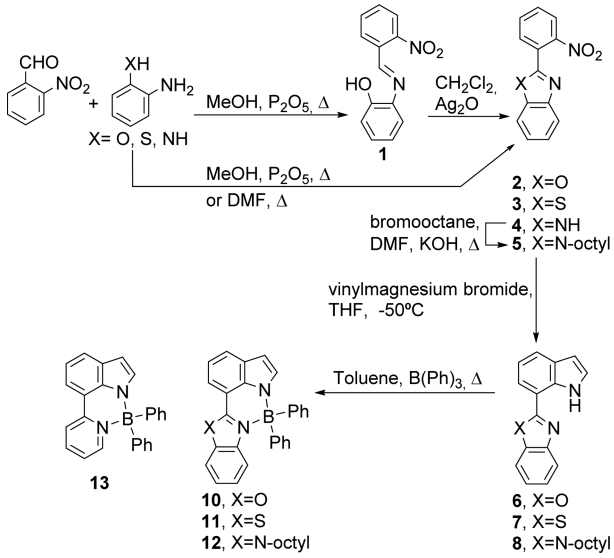

yl)indole, **9**, was synthesized according to reported methods.[12] The boron complexes, **10**–**13** were obtained by refluxing the indole-based ligands with triphenylborane in toluene solution. The full structural characterization of all the intermediate and final products was carried out by NMR spectroscopy and HRMS.

All the organoboron complexes showed a high thermal stability. The thermogravimetric analysis did not evidence any significant mass loss below the range 260–310 °C for the compounds **10**–**13** (Figure S16).

The solid state structure of some of the novel boron complexes, **10** and **12**, could be determined by single crystal X-ray diffraction (Figure S13). The differences observed in the solid state indicate the distinction in the electron donor ability of the heteroaromatic substructures and show the adequacy of our molecular design to modulate the electronic properties of the boron complexes.

Regarding the absorption spectroscopy, all the ligands showed two sets of bands within the ranges 235–245 and 325–350 nm, ascribed to π–π^* transitions (Figure 1A). The lower energy band in acetonitrile solution follows the trend **8** (317 nm) < **9** (323 nm) < **6** (345 nm) < **7** (354 nm), which falls below the lower limit of the visible radiation. Formation of the boron complexes causes a remarkable red shift of the absorption bands. These reach the visible range **12** (393 nm) < **13** (409 nm) < **10** (413 nm) < **11** (440 nm), and the complexes **10**–**13** become colored (Figure 1B). The electronic effects resulting upon coordination of the boron atom and the planarization of the π-conjugated ligand entail a narrowing of the energy gap between the ground state and the first singlet excited state. Apart from the mentioned band shift, the profile of the absorption spectra is very similar for the ligands and the boron complexes which reveals that the absorption bands are ligand-centered. At this point, it is worth noticing how a minor alteration in the structure of the heteroaromatic ligand enables a fine-tuning of the electronic properties in the synthesized boron complexes.

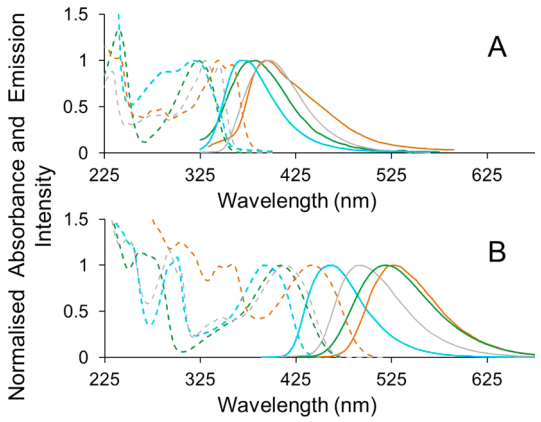

Figure 1. Absorption (dashed plot) and emission spectra (continuous plot) of ligands (A) and complexes (B) in CH_3CN (2×10^{-5} M). **6** and **10**, gray; **7** and **11**, orange; **8** and **12**, blue; **9** and **13**, green.

As far as the emission spectra are concerned, the ligands again reveal the effect of the heteroarene on the emission wavelength (Figure 1A). As expected, the fluorescence of the boron complexes is displaced toward longer wavelengths (460–530 nm). Whereas the ligands **6**–**9** show a very weak emission, the corresponding boron complexes **10**–**13** display a perceptible quantum yield enhancement, reaching a value of 44% in the case of the benzimidazole derivative **12** (Table 1). It is likely that the increase in the rigidity of the boron complex structure contributes to favor the radiative decay from the excited state. In this regard, the lifetime of the first excited state could be determined by fitting the TCSPC (Time Correlated Single Photon Counting) decay to a monoexponential model. Longer lifetimes are measured for the complexes with the benzoazaheteroaromatic systems **10**–**12** than with pyridine **13** (Table 1). Another property, which could spark interest in the applicability of the synthesized complexes as luminescent materials, is the moderate to large Stokes shifts detected,[13] reaching a value of 110 nm for compound **13**.

Additionally, the solvent effect on the optical properties of the boron complexes was studied in toluene, dichloromethane, ethanol, and acetonitrile (Figure S17). In general, all the compounds exhibited a subtle hypsochromic shift in their absorption bands upon increasing the solvent polarity. Conversely, the fluorescence spectra turned out to be much less sensitive to the solvent polarity with only a minor bathochromic shift being observed for compounds **10**, **11** and **13**. Accordingly, Lippert-Mataga plots revealed that compounds **10**–**13** have a very similar dipole moment both in the ground state and in the first singlet excited state (Figure S18; Table S3).[14] Thus, the measured Stokes shifts are ascribed to a structural reorganization in the excited state which does not necessarily imply a significant change in the dipole moment of the molecule.

With the aim of getting a better understanding about the electronic structure of the ligands and the boron complexes, their electrochemical characterization was also carried out. Cyclic voltammetry performed with compounds **6**–**9** displayed one-electron irreversible waves for all of them (Figure 2).

As it could be inferred from the comparison with the electrochemistry of plain indole, the redox process detected by cyclic voltammetry corresponded to the oxidation of the indole fragment in the structure of the ligand. Regarding the observed trend for the anodic peak potentials, **9** (1224 mV) < **8** (1266 mV) < indole (1342 mV) < **6** (1406 mV) < **7** (1469 mV), it evidenced the electron releasing effect of the pyridine and the *N*-octylbenzimidazole attached to the indole system. Con-

DOI: 10.1021/acs.joc.6b00265
J. Org. Chem. 2016, 81, 3296–3302

Table 1. Optical and Electrochemical Characterization

	6	7	8	9	10	11	12	13
$\lambda_{max.\ abs.}$ [nm] (ε)	345 (12×10^3)	354 (19×10^3)	317 (11×10^3)	323 (13×10^3)	413 (11×10^3)	440 (7.5×10^3)	393 (12×10^3)	409 (8×10^3)
Optical gap [eV]	3.40	3.26	3.35	3.44	2.64	2.44	2.65	2.63
$\lambda_{em.}$ [nm][a]	393	409	370	383	490	527	461	519
(Φ)[b]	(0.057)	(0.002)	(0.160)	(0.002)	(0.33)	(0.19)	(0.44)	(0.12)
τ (ns)[c]					11.04	11.29	8.80	1.20
E_{pa} [mV][d]	1406	1469	1266	1224	1367	1271	1199	1162
(E_{onset}) [mV]	(1210)	(1215)	(1110)	(1055)	(1220)	(1150)	(1090)	(1060)
LUMO [eV][e]	−2.15	−2.28	−2.10	−1.96	−2.92	−3.05	−2.78	−2.77
(theo) [eV][g]	(−1.70)	(−1.82)	(−1.38)	(−1.47)	(−2.26)	(−2.41)	(−1.92)	(−2.25)
HOMO [eV][f]	−5.55	−5.56	−5.45	−5.40	−5.56	−5.49	−5.43	−5.40
(theo) [eV][g]	(−5.76)	(−5.71)	(−5.59)	(−5.53)	(−5.67)	(−5.59)	(−5.51)	(−5.46)

[a] $\lambda_{exc\ (6)}$= 290 nm; $\lambda_{exc\ (7)}$= 240 nm; $\lambda_{exc\ (8)}$= 270 nm; $\lambda_{exc\ (9)}$= 280 nm; $\lambda_{exc\ (10)}$= 380 nm; $\lambda_{exc\ (11)}$= 410 nm; $\lambda_{exc\ (12)}$= 360 nm; $\lambda_{exc\ (13)}$= 370 nm. [b] Quantum yield determined in ethanol solution at room temperature using anthracene as reference. [c] Excited state lifetime;. [d] Anodic peak potential;. [e] $E_{LUMO} = E_{HOMO}$ + Optical gap. [f] Calculated as $E_{HOMO} = -(4.34 + E_{ox\ onset})$. [g] HOMO and LUMO energies determined by DFT.

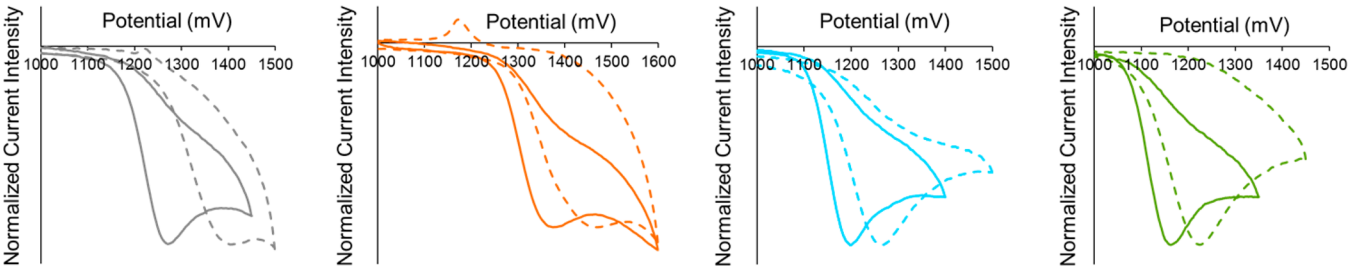

Figure 2. Cyclic voltammetry of the ligands (dashed plot) and the boron complexes (continuous plot) in CH_2Cl_2 (10^{-3} M), $TBAPF_6$ (0.1 M), T = 25 °C; scan rate, 100 mV/s; reference electrode, SCE; working electrode, Pt. **6** and **10**, gray; **7** and **11**, orange; **8** and **12**, blue; **9** and **13**, green.

versely, the benzoxazole and benzothiazole exerted an electron withdrawing effect over the indole system that consequently oxidized at higher potentials. As far as the cyclic voltammetry of the boron complexes **10**−**13** is concerned, an irreversible behavior was also observed and they maintained the previously discussed trend in their potentials but with a slight cathodic shift. Nonetheless, by correlating the onset value of the oxidation wave with the energy of the HOMO, we can conclude that the energies determined for the ligands **6**−**9** and the corresponding complexes **10**−**13** are almost identical (Table 1).[15] Approximating the HOMO−LUMO energy gap from the low energy onset in the absorption spectrum, we can indirectly estimate the LUMO energy using the electrochemically measured HOMO energy. Accordingly, a much lower LUMO is obtained for the complexes **10**−**13** than for the ligands **6**−**9**. Therefore, it can be concluded that complexation of the diphenylboron fragment mainly causes a stabilization of the LUMO, leaving the HOMO virtually unaffected.

The characterization of the compounds was further explored by computational methods, using DFT (Density Functional Theory) calculations. Regarding the orbital distribution (Figures 3 and S19), in the case of the ligands, although the HOMO is located over the whole conjugated system, a major contribution from the indole component is detected. Upon boron complexation, the location of the HOMO on the indole fragment is even more significant. These results are in good agreement with the previous discussion about the electrochemical oxidation being centered on the indole system. Moreover, an antibonding interaction is detected between the nitrogen π-orbitals in the ligand and the B−C_{phenyl} σ-bonds. This weak interaction becomes manifest in a minor increase of the HOMO energy of the boron complexes when compared to

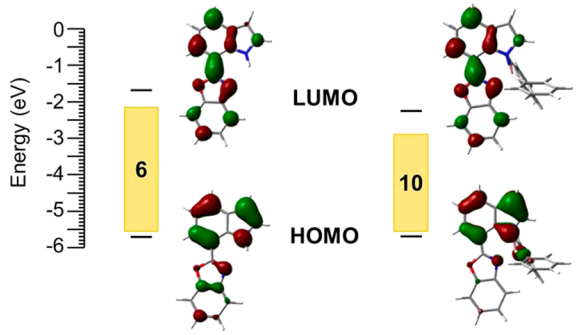

Figure 3. HOMO and LUMO energies (experimental, columns; theoretical, black dashes) and DFT isosurfaces exemplified for compounds **6** and **10**.

the DFT results of the corresponding ligands (Figure S19). Consequently, the subtly higher HOMO correlates well with the slight cathodic shift previously discussed. In any case, the DFT calculations confirmed a good consistency of the HOMO energies within the series **6**−**13**. Differently, the LUMO is distributed all over the conjugated system (Figures 3 and S19), with a lower contribution from the five-membered ring in the indole fragment. Considering the important contribution of the 7-azaheteroaryl component to the LUMO, the coordination of the boron atom by the nitrogen in the heteroaromatic component will result in a stabilization of the LUMO energy, as it has been experimentally observed.

Furthermore, TD-DFT (Time Dependent-DFT) calculations were also employed to confirm the identity of the electronic transitions in the absorption spectra (Table S4). Accordingly, the general behavior for the series of boron complexes could be

DOI: 10.1021/acs.joc.6b00265
J. Org. Chem. 2016, 81, 3296−3302

exemplified by the results obtained for the compound **10**. The calculations show a predicted absorption spectrum coincident with the experimental result. Three bands at 429, 369, and 286 nm are ascribed to the transitions between the energy states $S_0 \rightarrow S_1$, $S_0 \rightarrow S_2$, and $S_0 \rightarrow S_7$, respectively. In turn, the molecular orbital contribution to these transitions confirm the $\pi-\pi^*$ identity previously mentioned.

Due to the potential utility of the novel boron complexes as chromophores or fluorophores to be applied as materials in their solid state, the absorption and emission spectra were also studied for thin films prepared by spin-coating on quartz substrates (film thickness: 30−80 nm). As it can be observed in Figure S19, the absorption spectra are well overlapped with those obtained in solution, which implies that identical energy states are involved in the transitions. A slight red shift is more clearly detected for the complexes **9** and **10**, presumably due to intermolecular interactions in the solid state. Interestingly, when thin films are analyzed by emission spectroscopy, the spectral shift toward longer wavelengths is more significant. In agreement with these results, the technically appealing property of achieving long Stokes shifts is considerably enhanced for the samples in the solid state, with compounds **10**, **11**, and **13** showing values as large as 122, 125, and 129 nm, respectively. This larger energy shift even leads to a change in the color of the emitted light by the solid thin-film when compared to the color of the fluorescence in solution (Figure 4). The range of

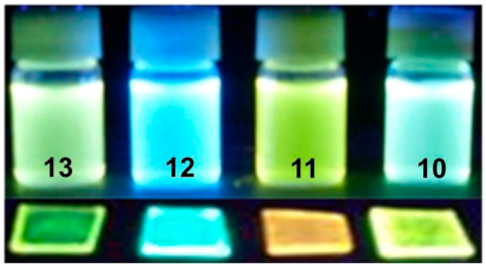

Figure 4. Fluorescence of boron complexes **10**−**13** in solution and thin films.

colors covered by the solid emission are **10**, orange; **11**, yellow-greenish; **12**, blue; and **13** green, which emphasizes the utility of the reported approach to achieve a fine-tuning of the emissive properties of four-coordinated boron complexes. Additionally, a remarkable quantum yield enhancement was obtained for the thin-films upon excitation at 360 nm: **10** (0.45), **11** (0.33), **12** (0.69), and **13** (0.23). These results also reinforce the potential applicability of some of these organoboron complexes as solid state light-emitters.

Besides, regarding the possible uses of these fluorophores and due to the relevant role that biocompatible organic dyes play in cell imaging, the boron complexes were studied in bioimaging experiments (Figure 5).

They permeated well into human breast cancer cells MCF7 (uptake time < 2 h) and, excepting compound **12**, they displayed low cytotoxicity (Figure S21). Cellular staining was studied by confocal microscopy at different excitation wavelengths. The images demonstrated that the delivered exogenous compounds are predominantly located in the perinuclear area, probably associated with endocytic vesicles.

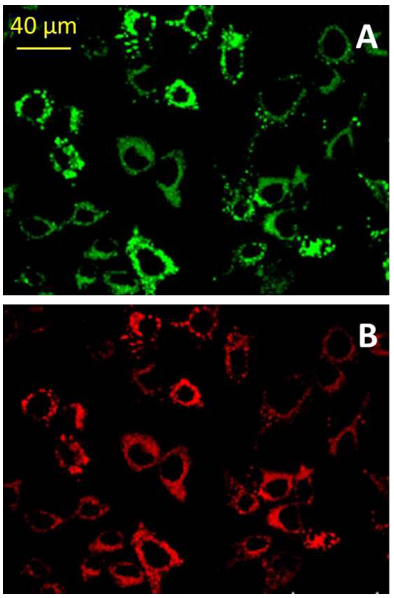

Figure 5. Confocal microscopy images (A, λ_{exc}= 488 nm; B, λ_{exc}= 561 nm) of human breast cancer cells MCF7 with fluorophore **11**.

CONCLUSION

In summary, a new series of organoboron complexes have been obtained via a simple synthetic route of 7-(azaheteroaryl)indole ligands. A fine modulation of the electronic structure has been achieved by modifying one heteroatom in the structure of the ligand which subsequently enabled the emission of fluorescence with a range of different colors. Large Stokes shifts have been detected in solution but, more importantly, in the solid state, reinforcing the interest of the organoboron species as emissive materials. The fluorescent properties of the four-coordinate boron complexes have proved to be useful in human breast cancer cell bioimaging.

EXPERIMENTAL SECTION

General Methods. Reagents used as starting materials were purchased from commercial sources and were used without further purification. Solvents were dried following the usual protocols (THF, Et_2O, and toluene were distilled from sodium wire with benzophenone indicator; CH_3CN and CH_2Cl_2 were distilled from $CaCl_2$; EtOH and MeOH were distilled from magnesium and stored with molecular sieves). Unless stated otherwise, all reactions were carried out under nitrogen atmosphere. Column chromatography was run with silica gel 60 A CC 70−200 μm as stationary phase, using HPLC grade solvents. Melting points are not corrected. Unless stated otherwise, all spectra were recorded at room temperature. ^{1}H NMR and ^{13}C NMR spectra were recorded on spectrometers having frequencies of 200, 300, or 400 MHz, for proton nuclei and 50, 75, or 100 MHz, respectively, for carbon nuclei. Chemical shifts are referred to the residual peak from the deuterated solvent. Mass spectrometry was recorded on HPLC−MS TOF instrument. Thermogravimetric analysis was carried out at a heating rate of 10 °C/min under nitrogen. Absorption spectra were recorded on a UV−vis-NIR spectrophotometer equipped with a Tungsten halogen visible source with quartz window and a deuterium arc UV source. A Hg lamp module was used as standard for automatic wavelength accuracy validation. Emission spectra were recorded on a fluorescence spectrophotometer with a Xe lamp as an excitation source. TCSPC experiments were carried out in a spectrophotometer, with a pulsed nanoLED ($\lambda_{exc.}$ = 372 nm), double slit monochromator, and photomultiplier TBX-04. The thin-film thicknesses were measured with a profilometer. Solid state quantum yields were measured at room temperature, using a xenon light source (150 W) and an integrating

DOI: 10.1021/acs.joc.6b00265
J. Org. Chem. 2016, 81, 3296−3302

sphere (3.3 in.). Electrochemistry was recorded using platinum electrodes as working and counter-electrode and Ag/AgCl or SCE as reference electrode. Decamethylferrocene or ferrocene was used as internal reference. Quantum chemical calculations were performed with the ORCA electronic structure program package.[16] All geometry optimizations were run in redundant internal coordinates with tight convergence criteria, using the B3LYP functional together with the new efficient RIJCOSX algorithm and the def2-TZVP basis set. Solvent effects (CH_2Cl_2) were taken into account via the COSMO solvation model. From these geometries, all reported data were obtained by means of single-point (SP) calculations using the same functional and the more polarizeddef2-TZVPP basis set. Reported energies are uncorrected for the zero-point vibrational term. A semiempirical correction accounting for the major part of the contribution of dispersion forces to the energy was included.

X-ray Structure Determination. Compound **10**: crystals suitable for X-ray experiments were obtained by evaporation from $CHCl_3$, $C_{27}H_{19}BN_2O$, M = 398.25, triclinic, $P\bar{1}$, a = 10.4924(4), b = 10.6628(4), c = 18.4160(4) Å, a = 74.5955(19)°, b = 84.469(2)°, g = 89.0236(13)°, U = 1977.01(12) Å^3, T = 120(1) K, Z = 4, 11 869 reflections measured, 8520 unique (R_{int} = 0.0371), hydrogen atoms refined as *riding*, two independent molecules in the asymmetric unit, R1 ($I > 2s(I)$) = 0.0547 and wR2 (all data) = 0.1396. Compound **12**: single crystals suitable for X-ray experiments were obtained by recrystallization from $CHCl_3$/pentane. $C_{35}H_{36}BN_3$, M = 509.48, orthorhombic, *Pbca*, a = 12.742(3), b = 14.710(3), c = 29.880(6) Å, U = 5600.9(19) Å^3, T = 120(1) K, Z = 8, 16 954 reflections measured, 4947 unique (R_{int} = 0.1764). Methyl hydrogen atoms refined as *rigid*, others *riding*. Despite the low ratio of observed/unique reflections, the structure refined to a C−C bond precision of 0.0087 Å, with R1 ($I > 2s(I)$) = 0.1087 and wR2 (all data) = 0.3150. CCDC-1449799 and CCDC-1449800 (www.ccdc.cam.ac.uk/data_request/cif).

Cell Cultures and Apoptosis Assays. The human cancer cell line MCF7 was obtained from the American Type Culture Collection (ATCC) and were maintained in appropriate culture media supplemented with 10% fetal calf serum and antibiotics under standard tissue culture conditions. Cell viability was evaluated by a colorimetric assay for mitochondrial function using the 3-(4,5-dimethylthiazol-2-yl)-2,5-diphenyltetrazolium bromide cell proliferation assay. For this assay, cells were plated in a 96-well plate at a density of 1000−2000 cells per well. Compounds were added once at the beginning of each experiment. The Hoechst staining method was used to detect apoptosis. Replicate cultures of 1 × 10^5 cells per well were plated in 6-well plates. The cells were subjected to the specified treatments for 72 h. After the medium was exchanged for fresh medium, the cells were incubated with 5 μL of Hoechst 33342 solution per well at 37 °C for 10 min and then observed under a fluorescence microscope. Strong fluorescence was observed in the nuclei of apoptotic cells, while weak fluorescence was observed in nonapoptotic cells. Quantification of the apoptotic cells was performed by counting the cells in four random fields in each well.

Microscopy. The imaging of organoboron compounds in live cells was performed using a confocal microscope. Images were collected following specific laser excitation and appropriated emission filters. Before live confocal microscopy, the cells were incubated in serum free Dulbecco's modified Eagle's medium (DMEM) for 1 h with organoboron compounds. After this time, the cells were extensively washed with DMEM. During imaging, the cells were incubated on a heated stage at 37 °C in DMEM. Images were processed with different software packages.

2-[(2-Nitrobenzylidene)amino]phenol, 1. A solution of 2-nitrobenzaldehyde (1 g, 9.16 mmol), 2-aminophenol (1.38 g, 9.16 mmol), and P_2O_5 (0.13 g, 10 mol %) in methanol (50 mL) under nitrogen atmosphere was refluxed for 48 h. Once the reaction was concluded, the crude was cooled to room temperature and the solvent was evaporated under vacuum. Then, the crude was dissolved in ethyl acetate, washed with water, dried over anhydrous Na_2SO_4, and concentrated by rotary evaporation. The resulting residue was treated with diethyl ether to obtain **1** as a yellow solid (1.65 g, 80%). Mp: 95−98 °C. ^{1}H NMR (400 MHz, $CDCl_3$) δ 6.94−6.97 (m, 1H), 7.03 (dd, J_1 = 4 Hz, J_2 = 1.2 Hz, 1H), 7.14 (s, 1H), 7.24−7.28 (m, 1H), 7.34−7.37 (m, 1H), 7.62−7.66 (m, 1H), 7.73−7.77 (m, 1H), 8.06−8.08 (m, 1H), 8.25−8.28 (m, 1H), 9.17 (s, 1H). ^{13}C NMR (50 MHz, $CDCl_3$) δ 115.4, 116.3, 120.3, 124.6, 129.5, 130.2, 130.5, 131.4, 133.4, 134.6, 149.3, 152.0, 152.7. HRMS (ESI-TOF) m/z: [M + H]$^+$ Calcd for $C_{13}H_{10}N_2O_3$ 243.0764. Found: 243.0772.

2-(2-Nitrophenyl)benzoxazole, 2. Ag_2O (1.48 g, 6.40 mmol) was added over a solution of 2-[(2-nitrobenzylidene]amino)phenol, **1**, (0.5 g, 2.07 mmol) in dichloromethane, and the resulting mixture was refluxed for 24 h. Then, the reaction mixture was allowed to cool down, the excess of Ag_2O was removed by filtration, and the solvent was evaporated under reduced pressure. The crude was subject to silica gel column chromatography eluting with ethyl acetate/*n*-hexane (1:1) to afford the pure title compound (0.31 g, 62%) as a yellow solid. R_f: 0.61. Mp: 99−102 °C. ^{1}H NMR (300 MHz, $CDCl_3$) δ 7.39−7.42 (m, 2H), 7.57−7.60 (m, 1H), 7.67−7.78 (m, 2H), 7.81−7.84 (m, 1H), 7.90 (dd, J_1= 7.8 Hz, J_2 = 1.5 Hz, 1H), 8.15 (dd, J_1= 7.2 Hz, J_2 = 1.8 Hz, 1H). ^{13}C NMR (75 MHz, $CDCl_3$) δ 110.9, 120.7, 121.4, 124.2, 124.9, 126.0, 131.4, 131.8, 132,3, 141.5, 149.2, 151.0, 158.8. HRMS (ESI-TOF) m/z: [M + H]$^+$ Calcd for $C_{13}H_9N_2O_3$ 241.0608. Found: 241.0615.

2-(2-Nitrophenyl)benzothiazole, 3. Over a solution of 2-nitrobenzaldehyde (1.21 g, 7.99 mmol) in methanol, 2-aminothiophenol (1 g, 7.99 mmol) and P_2O_5 (113.4 mg, 10 mol %) were successively added. The resulting mixture was refluxed for 48 h. Once the reaction was concluded, the crude was cooled to room temperature and the solvent was evaporated under vacuum. Then, the residue was dissolved in ethyl acetate, washed with water, dried over anhydrous Na_2SO_4, and concentrated by rotary evaporation. The resulting crude was purified by silica gel column chromatography using dichloromethane/hexane (1:1) as eluent to afford the pure expected compound as a yellow solid (0.5 g, 30%). R_f: 0.35. Mp: 120−122 °C. ^{1}H NMR (300 MHz,$CDCl_3$) δ 7.43−7.46 (m, 1H), 7.48−7.56 (m, 1H), 7.64 (td, J_1 = 7.8 Hz, J_2 = 1.8 Hz, 1H), 7.71 (td, J_1 = 7.5 Hz, J_2 = 1.5 Hz, 1H), 7.79−7.82 (m, 1H), 7.92−7.96 (m, 2H), 8.07−8.10 (m, 1H). ^{13}C NMR (50 MHz, $CDCl_3$) δ 121.5, 123.9, 124.5, 125.8, 126.5, 128.1, 130.9, 131.8, 132.3, 135.8, 148.9, 153.5, 162.3. HRMS (ESI-TOF) m/z: [M + H]$^+$ Calcd for $C_{13}H_8N_2O_2S$ 257.0379. Found: 257.0390.

2-(2-Nitrophenyl)benzimidazole, 4. *o*-Phenylenediamine (1.09 g, 10.0 mmol) was added over a solution of 2-nitrobenzaldehyde (1 g, 6.62 mmol) in dimethylformamide (50 mL), and the resulting mixture was stirred at 120 °C under nitrogen atmosphere for 14 h. The reaction was cooled to room temperature and the solvent was removed under reduced pressure. The resulting crude was treated with diethyl ether to obtain a pale brown precipitate which corresponds to the pure title compound (1 g, 63%). Mp: 259−262 °C. ^{1}H NMR (400 MHz, DMSO-d_6) δ 7.24 (bs, 2H), 7.58 (bs, 1H), 7.64 (bs, 1H), 7.73−7.77 (m, 1H), 7.84−7.88 (m, 1H), 7.97 (d, J = 8 Hz, 1H), 8.02 (d, J = 8 Hz, 1H), 13.05 (s, 1H). ^{13}C NMR (75 MHz, DMSO-d_6) δ 121.7, 129.3, 131.9, 133.1, 134.3, 140.9, 141.0, 142.6, 144.7, 153.6, 157.4, 159.0.HRMS (ESI-TOF) m/z: [M + H]$^+$ Calcd for $C_{13}H_{10}N_3O_2$ 240.0768. Found: 240.0772.

2-(2-Nitrophenyl)-1-octylbenzimidazole, 5. Over a solution of 2-(2-nitrophenyl)benzimidazole were sequentially added **4** (2 g, 8.36 mmol) in dimethylformamide (30 mL) at room temperature, potassium hydroxide (1.41 g, 25.08 mmol), and 1-bromooctane (8.08 g, 41.8 mmol). The resulting mixture was stirred at 100 °C for 10 h. After it had cooled at room temperature, the solvent was removed by rotary evaporation and the resulting residue was purified by column chromatography on silica gel eluting with ethyl acetate/hexane (2:1) to obtain **5** (2.11 g, 72%) as a yellow oil. R_f: 0.62. ^{1}H NMR (300 MHz, DMSO-d_6) δ 0.79 (t, J = 6.9 Hz, 3H), 1.09−1.19 (m, 10H), 1.62 (quint, J = 7.2 Hz, 2H), 4.14 (t, J = 7.5 Hz, 2H), 7.22−7.27 (m, 1H), 7.29−7.35 (m, 1H), 7.64 (d, J = 6.3 Hz, 1H), 7.68 (d, J = 7.8 Hz, 1H), 7.85−7.93 (m, 3H), 8.21−8.25 (m, 1H). ^{13}C NMR (75 MHz, DMSO-d_6) δ 13.9, 21.9, 25.8, 28.2, 28.3, 28.8, 31.0, 43.7, 110.9, 119.3, 121.9, 122.7, 124.8, 125.1, 131.4, 132.1, 133.6, 135.0, 142.5, 148.6, 149.0. HRMS (ESI-TOF) m/z: [M + H]$^+$ Calcd for $C_{21}H_{25}N_3O_2$ 352.2020. Found: 352.2025.

DOI: 10.1021/acs.joc.6b00265
J. Org. Chem. 2016, 81, 3296−3302

2-(Indol-7-yl)benzoxazole, 6. Vinylmagnesium bromide (18 mL, 12.5 mmol) was added dropwise over a solution of **2** (1.5 g, 6.25 mmol) in dry THF (50 mL) at −50 °C under nitrogen atmosphere. The reaction mixture was stirred at this temperature for 48 h. Then, a saturated aqueous solution of NH_4Cl (50 mL) was added, and the crude was allowed to reach room temperature. The solvent was evaporated by rotary evaporation, and the reaction crude was extracted with diethyl ether (3 × 70 mL). The combined organic layers were washed with a saturated aqueous solution of NH_4Cl (100 mL), water (100 mL), and brine (100 mL) and dried over anhydrous Na_2SO_4, and the solvent was evaporated under reduced pressure. The crude was purified by silica gel column chromatography eluting with dichloromethane/hexane (1:1) to obtain **6** (450 mg, 30%) as a yellow solid. R_f: 0.77. Mp: 140−142 °C. ^{1}H NMR (300 MHz, $CDCl_3$) δ 6.65−6.67 (m, 1H), 7.23−7.29 (m, 2H), 7.35−7.38 (m, 2H), 7.42−7.43 (m, 1H), 7.61−7.64 (m, 1H), 7.77−7.80 (m, 1H), 7.85 (dd, J_1 = 7.8 Hz, J_2 = 0.6 Hz, 1H), 8.04−8.06 (m, 1H), 10.73 (s, 1H). ^{13}C NMR (75 MHz, $CDCl_3$) δ 102.8, 109.8, 110.6, 119.5, 121.2, 124.5, 124.8, 124.9, 125.3, 128.7, 134.0, 142.1, 150.0, 162.6. HRMS (ESI-TOF) m/z: $[M + H]^+$ Calcd for $C_{15}H_{10}N_2O$ 235.0866, Found: 235.0874.

2-(Indol-7-yl)benzothiazole, 7. A solution of 2-(2-nitrophenyl)-benzothiazole, **3** (1.5 g, 6 mmol), in dry THF (50 mL) was cooled to −50 °C under nitrogen atmosphere. At this temperature, vinylmagnesium bromide (17 mL, 12 mmol) was added dropwise and the resulting mixture was stirred for 48 h. The evolution of the reaction was followed by thin layer chromatography, and once completed, a saturated aqueous solution of NH_4Cl (50 mL) was added and the crude was allowed to reach room temperature. The solvent was evaporated by rotary evaporation, and the reaction crude was extracted with diethyl ether (3 × 70 mL). The combined organic layers were washed with a saturated aqueous solution of NH_4Cl (100 mL), water (100 mL), and brine (100 mL) and dried over anhydrous Na_2SO_4, and the solvent was evaporated under reduced pressure. The crude was purified by silica gel column chromatography eluting with dichloromethane/hexane (1:3) to isolate **7** (0.53 g, 35%) as a yellow solid. R_f: 0.52. Mp: 112−114 °C. ^{1}H NMR (400 MHz, $CDCl_3$) δ 6.66−6.67 (m, 1H), 7.20−7.26 (m, 1H), 7.38−7.45 (m, 1H), 7.50−7.53 (m, 1H), 7.77 (d, J = 7.5 Hz, 1H), 7.82 (d, J = 7.5 Hz, 1H), 7.93 (d, J = 7.8 Hz, 1H), 8.09 (d, J = 7.8 Hz, 1H), 10.99 (s, 1H). ^{13}C NMR (50 MHz, $CDCl_3$) δ 102.4, 116.4, 119.4, 121.4, 122.0, 122.5, 124.0, 124.9, 125.3, 126.1, 128.9, 133.1, 133.6, 153.8, 167.9. HRMS (ESI-TOF) m/z: $[M + H]^+$ Calcd for $C_{15}H_{10}N_2S$ 251.0637. Found: 251.0640.

2-(Indol-7-yl)-1-octylbenzimidazole, 8. A solution of 2-(2-nitrophenyl)-1-octylbenzimidazole, **5** (1 g, 2.49 mmol), in dry THF (50 mL) was cooled to −50 °C under nitrogen atmosphere. At this temperature, vinylmagnesium bromide (12.21 mL, 8.55 mmol) was added dropwise and the resulting mixture was stirred for 48 h. The evolution of the reaction was followed by thin layer chromatography, and once completed, a saturated aqueous solution of NH_4Cl (50 mL) was added and the crude was allowed to reach room temperature. The solvent was evaporated by rotary evaporation, and the reaction crude was extracted with diethyl ether (3 × 70 mL). The combined organic layers were washed with a saturated aqueous solution of NH_4Cl (100 mL), water (100 mL), and brine (100 mL), and dried over anhydrous Na_2SO_4, and the solvent was evaporated under reduced pressure. The crude was purified by silica gel column chromatography eluting with ethyl acetate/hexane (1:1) to isolate the desired compound (0.30 g, 30.2%) as a brown oil. R_f: 0.70. ^{1}H NMR (400 MHz, $CDCl_3$) δ 0.89 (t, J = 6.9 Hz, 3H), 1.26−1.45 (m, 9H), 2.01 (quint, J = 7.2 Hz, 2H), 4.45 (t, J = 7.5 Hz, 2H), 6.64−6.66 (m, 1H), 7.24−7.28 (m, 1H), 7.33−7.37 (m, 2H), 7.38 (t, J = 2.8 Hz, 1H), 7.46−7.50 (m, 1H), 7.53 (d, J = 7.6 Hz, 1H), 7.80 (d, J = 8 Hz, 1H), 7.85−7.89 (m, 1H), 10.60 (s, 1H). ^{13}C NMR (100 MHz, $CDCl_3$) δ 14.0, 22.6, 26.8, 29.0, 29.1, 29.9, 31.7, 45.2, 102.4, 109.9, 113.1, 118.9, 119.4, 120.4, 122.3, 122.6, 122.7, 125.3, 129.0, 135.1, 135.7, 142.9, 151.4. HRMS (ESI-TOF) m/z: $[M + H]^+$ Calcd for $C_{23}H_{27}N_3$ 346.2278. Found: 346.2284.

(*N*^{3}-*B*)-2-[1-(Diphenylboryl)indol-7-yl]benzoxazole, 10. A solution of 2-(indol-7-yl)benzoxazole, **6** (0.50 g, 2.16 mmol), and triphenylborane (0.79 g, 3.24 mmol) in dry toluene (30 mL) under nitrogen atmosphere was refluxed for 48 h. The reaction mixture was cooled to room temperature, and the solvent was evaporated under reduced pressure. The crude was purified by silica gel column chromatography eluting with ethyl acetate/hexane (1:5) to afford the pure title compound (30 mg, 3%) as a yellow solid. R_f: 0.40. Mp: 227−229 °C. ^{1}H NMR (300 MHz, $CDCl_3$) δ 6.62 (d, J = 3 Hz, 1H), 7.18−7.42 (m, 15H), 7.67, (d, J = 8.1 Hz, 1H), 7.81 (d, J = 7.2 Hz, 1H), 7.95 (d, J = 7.8 Hz, 1H). ^{13}C NMR (75 MHz, $CDCl_3$) δ 102.7, 102.9, 103.5, 111.4, 117.9, 118.4, 118.6, 126.2, 126.6, 127.3, 128.7, 129.2, 132.5, 133.4, 139.1, 149.5, 162.0. ^{11}B-NMR (128.34 MHz, $CDCl_3$) δ 3.85 (s). HRMS (ESI-TOF) m/z: $[M + H]^+$ Calcd for $C_{27}H_{19}BN_2O$ 398.1700. Found: 398.1698.

(*N*^{3}-*B*)-2-[1-(Diphenylboryl)indol-7-yl]benzothiazole, 11. A mixture of 2-(indol-7-yl)benzothiazole, **7** (717 mg, 2.87 mmol), and triphenylborane (1.04 g, 4.31 mmol) in dry toluene (30 mL) under nitrogen atmosphere was heated at reflux temperature, and the reaction progress was followed by thin layer chromatography. Once the reaction was concluded (48 h), it was cooled to room temperature and the solvent was evaporated under vacuum. The crude was treated with diethyl ether to obtain a yellow solid (307 mg, 31%) which corresponds to the pure title compound. Mp: 229−232 °C. ^{1}H NMR (300 MHz) δ 6.55 (d, J = 2.7 Hz, 1H), 7.09−7.13 (m, 2H), 7.16−7.25 (m, 7H), 7.33−7.39 (m, 5H), 7.60 (d, J = 7.5 Hz, 1H), 7.75−7.83 (m, 2H), 7.86−7.88 (m, 1H). ^{13}C NMR (75 MHz, $CDCl_3$) δ 102.7, 111.0, 118.7, 118.9, 122.0, 122.5, 126.2, 126.5, 127.2, 127.4, 128.2, 129.4, 130.0, 132.6, 133.5, 135.8, 145.9, 168.9. ^{11}B-NMR (128.34 MHz, $CDCl_3$) δ 4.87 (s). HRMS (ESI-TOF) m/z: $[M + H]^+$ Calcd for $C_{27}H_{19}BN_2S$ 414.1471. Found: 414.1473.

(*N*^{3}-*B*)-2-[1-(Diphenylboryl)indol-7-yl]-1-octylbenzimidazole, 12. A mixture of **8** (245 mg, 0.71 mmol) and triphenylborane (258 mg, 1.07 mmol) in dry toluene (40 mL) under nitrogen atmosphere was heated at reflux temperature, and the reaction progress was followed by thin layer chromatography. Once the reaction was concluded (48 h), it was cooled to room temperature and the solvent was evaporated under vacuum. The residue was subjected to column chromatography on silica gel eluting with dichloromethane/hexane (1:1) to isolate **12** (136 mg, 38%) as a yellow solid. R_f: 0.71. Mp: 201−203 °C. ^{1}H NMR (400 MHz, $CDCl_3$) δ 0.92 (t, J = 6.9 Hz, 3H), 1.26−1.63 (m, 10H), 2.12 (quint, J = 7.2 Hz, 2H), 4.66 (t, J = 7.5 Hz, 2H), 6.60 (d, J = 2.8 Hz, 1H), 7.12−7.20 (m, 9H), 7.26−7.35 (m, 8H), 7.45 (d, J = 8 Hz, 1H), 7.64 (d, J = 7.6 Hz, 1H), 7.86 (d, J = 7.6 Hz, 1H). ^{13}C NMR (75 MHz, $CDCl_3$) δ 14.1, 22.6, 26.9, 29.1, 29.1, 31.7, 46.3, 102.2, 107.0, 109.8, 116.9, 118.1, 118.7, 124.4, 125.9, 126.1, 127.1, 129.9, 132.4, 133.5, 134.4, 135.0, 138.2, 146.7. ^{11}B-NMR (128.34 MHz, $CDCl_3$) δ 3.67 (s). HRMS (ESI-TOF) m/z: $[M + H]^+$ Calcd for $C_{35}H_{36}BN_3$ 509.3111. Found: 509.3112.

(*N*^{1}-*B*)-7-[1-(Diphenylboryl)pyrid-2-yl]indole, 13. A mixture of 7-(2-pyrid-2-yl)indole (76.2 mg, 0.39 mmol) and triphenylborane (95 mg, 0.39 mmol) in dry toluene (30 mL) under nitrogen atmosphere was refluxed for 48 h. Then, the reaction mixture was allowed to reach room temperature and the solvent was evaporated by rotary evaporation. The remaining residue was purified by preparative thin layer chromatography using dichloromethane/hexane (2:1) as eluent to obtain **13** as a pure yellow solid (58 mg, 41%). R_f: 0.66. Mp: 211−213 °C. ^{1}H NMR (300 MHz, $CDCl_3$) δ 6.59 (d, J = 2.8 Hz, 1H), 7.10−7.23 (m, 13H), 7.67 (d, J = 7.6 Hz, 1H), 7.81 (d, J = 8 Hz, 1H), 7.94−7.98 (m, 1H), 8.25 (d, J = 8 Hz, 1H), 8.46−8.48 (m, 1H). ^{13}C NMR (75 MHz, $CDCl_3$) δ 101.9, 113.6, 116.6, 118.70, 120.6, 121.6, 125.5, 126.5, 127.4, 129.9, 132.2, 133.4, 136.3, 140.1, 146.2, 151.9. ^{11}B-NMR (128.34 MHz, $CDCl_3$) δ 4.00 (s). HRMS (ESI-TOF) m/z: $[M + H]^+$ Calcd for $C_{25}H_{19}BN_2$ 358.1756. Found: 358.1750.

■ ASSOCIATED CONTENT

Supporting Information

The Supporting Information is available free of charge on the ACS Publications website at DOI: 10.1021/acs.joc.6b00265.

NMR spectra; X-ray structures; thermogravimetric analysis; cyclic voltammetry; TD-DFT calculations; solvent effects; Lippert-Mataga plots; thin film absorp-

DOI: 10.1021/acs.joc.6b00265
J. Org. Chem. 2016, 81, 3296−3302

tion and emission spectra; Cell cultures and apoptosis assays (PDF)
Crystallographic data for compound **10** (CIF)
Crystallographic data for compound **12** (CIF)

AUTHOR INFORMATION

Corresponding Author

*E-mail: davidcc@um.es.

Notes

The authors declare no competing financial interest.

ACKNOWLEDGMENTS

This research has been funded by the Spanish Ministry of Economy and Competitivity (Projects: (D.C. and A.T.) CTQ2014-58875-R; (J.N.R.-L.) SAF2013-48375-C2-1-R) and Fundación Séneca Región de Murcia (Project: (J.N.R.-L.) 15230/PI/10 and 19304/PI/14). A.E.F. thanks the resources from Servicio de Cálculo Científico (University of Murcia), as well as the financial support from COST action CM1302.

REFERENCES

(1) (a) Li, D.; Zhang, H.; Wang, Y. *Chem. Soc. Rev.* **2013**, *42*, 8416. (b) Rao, Y.-L.; Wang, S. *Inorg. Chem.* **2011**, *50*, 12263.

(2) (a) Duran-Sampedro, G.; Esnal, I.; Agarrabeitia, A. R.; Bañuelos Prieto, J.; Cerdán, L.; García-Moreno, I.; Costela, A.; Lopez-Arbeloa, I.; Ortiz, M. J. *Chem. - Eur. J.* **2014**, *20*, 2646. (b) Costela, A.; García-Moreno, I.; Pintado-Sierra, M.; Amat-Guerri, F.; Sastre, R.; Liras, M.; Arbeloa, F. L.; Prieto, J. B.; Arbeloa, I. L. *J. Phys. Chem. A* **2009**, *113*, 8118.

(3) (a) Singh, S. P.; Gayathri, T. *Eur. J. Org. Chem.* **2014**, *2014*, 4689. (b) Bessette, A.; Hanan, G. S. *Chem. Soc. Rev.* **2014**, *43*, 3342.

(4) (a) Kowada, T.; Maeda, H.; Kikuchi, K. *Chem. Soc. Rev.* **2015**, *44*, 4953. (b) Ni, Y.; Wu, J. *Org. Biomol. Chem.* **2014**, *12*, 3774. (c) Shaikh, A. C.; Ranade, D. S.; Thorat, S.; Maity, A.; Kulkarni, P. P.; Gonnade, R. G.; Munshi, P.; Patil, N. T. *Chem. Commun.* **2015**, *51*, 16115.

(5) (a) Kamkaew, A.; Lim, S. H.; Lee, H. B.; Kiew, L. V.; Chung, L. Y.; Burgess, K. *Chem. Soc. Rev.* **2013**, *42*, 77. (b) Banfi, S.; Caruso, E.; Zaza, S.; Mancini, M.; Gariboldi, M. B.; Monti, E. *J. Photochem. Photobiol., B* **2012**, *114*, 52. (c) Awuah, S. G.; You, Y. *RSC Adv.* **2012**, *2*, 11169.

(6) (a) Misra, R.; Jadhav, T.; Dhokale, B.; Mobin, S. M. *Dalton Trans.* **2015**, *44*, 16052. (b) Ashokkumar, P.; Weißhoff, H.; Kraus, W.; Rurack, K. *Angew. Chem., Int. Ed.* **2014**, *53*, 2225. (c) Kim, H. N.; Ren, W. X.; Kim, J. S.; Yoon, J. *Chem. Soc. Rev.* **2012**, *41*, 3210. (d) Boens, N.; Leen, V.; Dehaen, W. *Chem. Soc. Rev.* **2012**, *41*, 1130.

(7) (a) Ulrich, G.; Ziessel, R.; Harriman, A. *Angew. Chem., Int. Ed.* **2008**, *47*, 1184. (b) Ziessel, R.; Ulrich, G.; Harriman, A. *New J. Chem.* **2007**, *31*, 496. (c) Loudet, A.; Burgess, K. *Chem. Rev.* **2007**, *107*, 4891.

(8) Frath, D.; Massue, J.; Ulrich, G.; Ziessel, R. *Angew. Chem., Int. Ed.* **2014**, *53*, 2290.

(9) Gribble, G. W. *J. Chem. Soc., Perkin Trans. 1* **2000**, 1045.

(10) (a) Curiel, D.; Más-Montoya, M.; Usea, L.; Espinosa, A.; Orenes, R. A.; Molina, P. *Org. Lett.* **2012**, *14*, 3360. (b) Liu, Q.-D.; Mudadu, M. S.; Thummel, R.; Tao, Y.; Wang, S. *Adv. Funct. Mater.* **2005**, *15*, 143. (c) Liu, Q.; Mudadu, M. S.; Schmider, H.; Thummel, R.; Tao, Y.; Wang, S. *Organometallics* **2002**, *21*, 4743. (d) Liu, S.-F.; Wu, Q.; Schmider, H. L.; Aziz, H.; Hu, N.-X.; Popović, Z.; Wang, S. *J. Am. Chem. Soc.* **2000**, *122*, 3671.

(11) Bartoli, G.; Palmieri, G.; Bosco, M.; Dalpozzo, R. *Tetrahedron Lett.* **1989**, *30*, 2129.

(12) Mudadu, M. S.; Singh, A.; Thummel, R. P. *J. Org. Chem.* **2006**, *71*, 7611.

(13) (a) Er, J. C.; Tang, M. K.; Chia, C. G.; Liew, H.; Vendrell, M.; Chang, Y.-T. *Chem. Sci.* **2013**, *4*, 2168. (b) Chen, Y.; Zhao, J.; Guo, H.; Xie, L. *J. Org. Chem.* **2012**, *77*, 2192.

(14) Reichardt, C. *Solvents and Solvent Effects in Organic Chemistry*; Wiley-VCH: Weinheim, 2003.

(15) (a) Loutfy, R. O. *J. Chem. Phys.* **1977**, *66*, 4781. (b) Parker, V. D. *J. Am. Chem. Soc.* **1976**, *98*, 98.

(16) ORCA—an ab initio, density functional and semiempirical program package. Written by F. Neese. Version 2.8.0, Universität Bonn, 2010. Web page: http://www.thch.uni-bonn.de/tc/orca/.

DOI: 10.1021/acs.joc.6b00265
J. Org. Chem. 2016, 81, 3296−3302